Investigation of the negative-mass behaviors occurring below a cut-off frequency

2010 New J. Phys. 12 103025

(http://iopscience.iop.org/1367-2630/12/10/103025)

New Journal of Physics
The open-access journal for physics

Investigation of the negative-mass behaviors occurring below a cut-off frequency

Shanshan Yao, Xiaoming Zhou[1] and Gengkai Hu[1]
School of Aerospace Engineering, Beijing Institute of Technology, Beijing 100081, People's Republic of China
E-mail: zhxming@bit.edu.cn and hugeng@bit.edu.cn

New Journal of Physics **12** (2010) 103025 (13pp)
Received 9 July 2010
Published 14 October 2010
Online at http://www.njp.org/
doi:10.1088/1367-2630/12/10/103025

Abstract. Negative-mass phenomena occurring below a cut-off frequency are examined using both theoretical and experimental methods. The paper begins with an investigation of a mass–spring structure, the effective mass of which is shown to be negative below a specific frequency. Due to the decaying nature of lattice waves in the negative-mass system, the transmission drop induced by negative effective mass is demonstrated experimentally. Further investigation is conducted for a rectangular solid waveguide with clamped boundary conditions. It is shown that the lowest bandgap mode of the clamped waveguide can be attributed to negative effective mass below a cut-off frequency. Based on this observation, elastic metamaterials made of a steel grid filled with styrene butadiene rubber are designed and fabricated. Both the simulation and experimental analyses demonstrate that the designed metamaterials have negative effective mass below a cut-off frequency.

[1] Authors to whom any correspondence should be addressed.

Contents

1. Introduction

Metamaterials with anomalous physical properties have received much attention from the scientific community in recent years and have also stimulated many important concepts for potential engineering applications, such as super-resolution imaging [1, 2] and cloaking [3, 4]. With tailored sub-wavelength microstructures, metamaterials possess negative effective parameters around resonant frequencies of their building blocks. In electromagnetics, a typical metamaterial is electric plasma, whose effective permittivity becomes negative below the plasma frequency. Periodically arranged metallic wires [5] and hollow metallic waveguides [6] are found to behave in this fashion at microwave frequencies. Another typical electromagnetic (EM) metamaterial is periodically distributed split-ring resonators (SRR) [7], having negative effective permeability in the finite bandwidth close to the resonant frequency of the SRR. For engineering applications, metamaterials with broadband negative material parameters are desired.

Analogous to EM metamaterials, acoustic/elastic metamaterials with negative effective mass can be realized. A well-known example is the composite made by filling an epoxy matrix with periodically arranged rubber-coated lead spheres [8]. The unusual low-frequency bandgaps observed in such a composite are attributed to negative effective mass, which is defined due to the out-of-phase motion between the resonant unit and the matrix material. This mechanism can be well understood by using either equivalent discrete mass–spring systems [9]–[11] or continuum analytic models [12, 13]. Recently, Yang *et al* [14, 15] proposed lightweight membrane-type metamaterials with negative effective mass in the low frequency regime. The structure consisted of a circular elastic membrane with a small weight attached at the center and the outer boundary being fixed. Although operating in the low frequency regimes, the aforementioned metamaterials show the negative-mass effect that is only available in a finite bandwidth around resonant frequencies. For engineering applications, there is a great demand for designing acoustic metamaterials with broadband negative parameters, especially at extremely low frequencies.

Due to the similarity between EM and acoustic wave phenomena, one can expect to design an acoustic metamaterial with negative effective mass below a cut-off frequency,

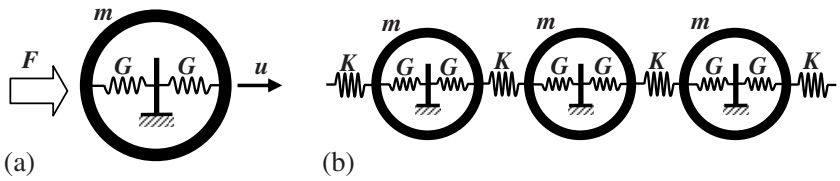

Figure 1. (a) The analyzed composite structure and (b) an infinite lattice system composed of structures that are connected by springs K.

analogous to the behavior of the electric plasma. Recently, Lee *et al* [16] reported an interesting experimental result; they demonstrated that a stretched rubber membrane with a fixed outer boundary can be homogenized as an acoustic metamaterial with negative effective mass below a critical frequency. In this paper, we further explore this phenomenon and demonstrate by both theoretical and experimental methods that such a property is not just limited to membrane-type materials.

The paper is organized as follows. In section 2, we propose a mass–spring system with negative effective mass below a specific frequency. The peculiar stopband effect due to negative mass is demonstrated by experiments. In section 3, rectangular waveguides with clamped boundary conditions are analyzed. The correlation between the bandgap modes of the clamped waveguide and negative effective mass is studied. In section 4, elastic metamaterials operative in the audible regime are designed based on the waveguide theory. Detailed simulation and experimental analyses are presented to demonstrate negative effective mass below the lowest eigenfrequency of the structure. The paper is summarized in section 5.

2. Negative effective mass below a cut-off frequency for a mass–spring system

2.1. Negative effective mass of a mass–spring structure

Consider a mass–spring structure, as shown in figure 1(a), where an outer mass m is confined by two elastic springs G. It is the case that the inner mass is fixed in the model examined by Yao *et al* [10]. Now connect such a structure by using springs K with spacing a apart to build a one-dimensional (1D) infinite lattice system, as shown in figure 1(b). The equilibrium equation for the nth mass, whose displacement is denoted by u_n, is

$$m\frac{\mathrm{d}^2u_n}{\mathrm{d}t^2} = K\,(u_{n-1}-u_n) - K\,(u_n-u_{n+1}) - 2Gu_n. \tag{1}$$

Assuming the harmonic time dependence $\mathrm{e}^{-\mathrm{i}\omega t}$ and use Bloch's condition $u_{n+1} = u_n\mathrm{e}^{\mathrm{i}qa}$ with q being the Bloch wave vector, the dispersion relation of the system is derived from equation (1) to be

$$\left(m-\frac{2G}{\omega^2}\right)\omega^2 = 4K\sin^2\frac{qa}{2}. \tag{2}$$

Comparing equation (2) with dispersion relation of a simple mass–spring lattice model, one can define an effective mass

$$m_{\mathrm{eff}} = m\left(1-\frac{\omega_0^2}{\omega^2}\right), \quad \omega_0 = \sqrt{\frac{2G}{m}}. \tag{3}$$

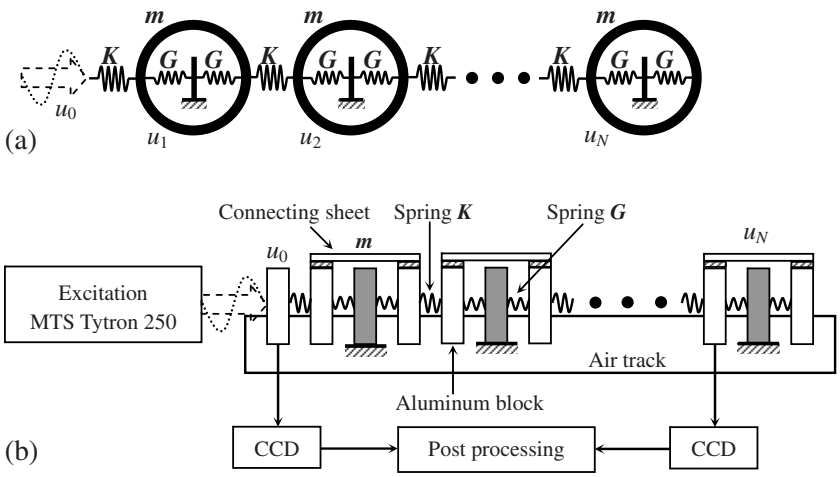

Figure 2. (a) The finite mass–spring lattice system and (b) the experimental realization for such a lattice system.

From equations (2) and (3), it is found that the proposed structure would give rise to a broadband negative effective mass below the frequency ω_0.

Alternatively, in figure 1(a), suppose that the mass m has a displacement u under a harmonic force F of angular frequency ω. Newton's law of motion gives the relation $F = -m_0\omega^2 u + 2Gu$ for the mass m. If the composite unit is considered to be a solid object with an effective mass m_{eff}, we have $F = -m_{\text{eff}}\omega^2 u$, with m_{eff} given by equation (3).

2.2. *Experimental validation*

Experimental validation is done by measuring the transmittance of a finite lattice system; low transmittance can give an indication of negative-effective mass [10]. For a finite lattice system involving N periods, as shown in figure 2(a), the transmittance T is defined to be u_N/u_0 and is given by

$$T \overset{\text{def}}{=} \prod_{n=1}^{N} T_n, \tag{4}$$

where $T_n = u_n/u_{n-1}$ is calculated by using the following recurrent relation,

$$T_n = \frac{K}{K(2-T_{n+1}) - m_{\text{eff}}\omega^2}, \quad n = 1, 2, \ldots, N, \tag{5}$$

with $T_{N+1} = 1$.

Measurements of the transmission for a seven-period system are made based on an air track-lifting system; see [10] for experimental details. The experimental realization of such a lattice system is shown in figure 2(b). Two aluminum blocks, together with a connecting sheet, realize the mass m. Springs G connect the mass to a fixed aluminum block that is placed inside the preceding composite unit, generating restrained forces on the mass m. In the experiment, the material parameters are $m = 101.10\,\text{g}$, $G = 37\,\text{N m}^{-1}$, and $K = 117\,\text{N m}^{-1}$. Figures 3(a) and (b) show, respectively, the dispersion curve and effective mass as a function of frequency according

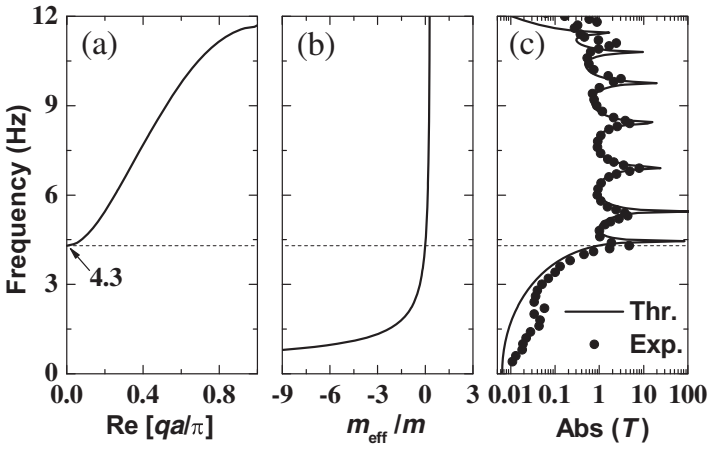

Figure 3. (a) The dispersion curve from equation (2), (b) normalized effective mass from equation (3) and (c) experimental and theoretical transmittances for a seven-period system.

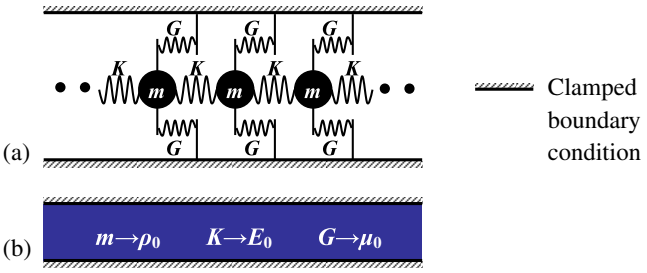

Figure 4. (a) The infinite lattice system completely equivalent to that shown in figure 1(b); (b) the proposed continuum material model: the solid waveguide with clamped boundaries where the mass density ρ_0, Young's modulus E_0 and shear modulus μ_0 of the material realize m, K and G of the lattice system, respectively.

to equations (2) and (3). It is seen that negative-effective mass occurs below 4.3 Hz and opens a large gap region in the dispersion curve. The measured transmittances for the seven-unit system are plotted in figure 3(c), together with the theoretical prediction given by equation (4). In figure 3(c), excellent agreement between the theoretical and experimental results can be seen. The results clearly show the transmission drop below 4.3 Hz, demonstrating the existence of negative effective mass below a cut-off frequency.

3. The negative-mass effect for a rectangular solid waveguide with clamped boundaries

3.1. The dispersion effect of clamped waveguides

In order to proceed, a lattice system that is completely equivalent to that shown in figure 1(b) is presented in figure 4(a). It suggests that a rectangular solid waveguide with clamped boundary conditions may have a dispersion characteristic similar to that of the lattice system proposed in section 2, since the mass density ρ_0, Young's modulus E_0 and shear modulus μ_0 of the solid material in the waveguide can realize the m, K and G of the lattice system, respectively. For the

clamped solid waveguide, it is known that there is a cut-off frequency below which no type of elastic wave is permitted. In the following, we will attribute this bandgap to negative-effective mass.

Consider a solid waveguide with a rectangular cross-section having x and y dimensions of a and b, and infinitely extended in the z-direction. When such waveguide has clamped boundary conditions, the dispersion relations of guided waves are given by [17]

$$\frac{\omega^2}{c_{\mathrm{d}}^2} = p^2 + \left(\frac{m\pi}{a}\right)^2 + \left(\frac{n\pi}{b}\right)^2, \quad m = 1, 2, \ldots, \quad n = 1, 2, \ldots, \tag{6a}$$

for P modes, and

$$\frac{\omega^2}{c_{\mathrm{s}}^2} = p^2 + \left(\frac{m\pi}{a}\right)^2 + \left(\frac{n\pi}{b}\right)^2, \quad m = 1, 2, \ldots, \quad n = 1, 2, \ldots, \tag{6b}$$

for S modes, where c_{d} and c_{s} are, respectively, the wave velocities of P and S waves, and p is the propagation constant along the z-direction. For conventional elastic materials, the shear wave velocity c_{s} is always less than the longitudinal wave velocity c_{d}. Therefore, the dispersion relation (6) will lead to a lowest cut-off frequency $\omega_{\mathrm{c}} = c_{\mathrm{s}}\sqrt{(\pi/a)^2 + (\pi/b)^2}$, below which there are neither propagating P nor S waves since the propagation constant p will take purely imaginary values. We consider this clamped waveguide as a homogenized material with mass density ρ_{eff}, Young's modulus E_0 and shear modulus μ_0; its dispersion relation can be written as $p = \omega\sqrt{\rho_{\mathrm{eff}}/\mu_0}$. According to equation (6*b*) and taking $m = 1$ and $n = 1$, a theoretical prediction of the effective mass density ρ_{eff} can be given by

$$\rho_{\mathrm{eff}} = \rho_0\left(1 - \frac{\omega_{\mathrm{c}}^2}{\omega^2}\right). \tag{7}$$

Equation (7) should be valid in the frequency range where the second branch for either S or P mode is not involved. This phenomenon is the elastic wave counterpart of the bandgap effect occurring in the hollow metallic waveguides for EM waves, which can be explained by negative-effective permittivity [6].

3.2. Numerical validation for negative mass in a clamped waveguide

In order to verify the effective mass defined by equation (7) for the solid waveguide with fixed boundary conditions, we perform numerical simulations for a finite-thickness slab with clamped boundaries. To compute the sound transmission, the slab is sandwiched by two semi-infinite fluid materials loaded in the waveguide, as shown in figure 5. The lateral boundaries of the waveguide are clamped for the elastic slab and rigid for the fluids. Modeling is performed using COMSOL Multiphysics. The plane harmonic wave is incident from the left side of the waveguide. The fluid–structure coupling boundary conditions are set at the interfaces between the elastic slab and fluid; the radiation boundary conditions are applied on the entrance and exit faces of the waveguide to simulate the infinite extent environment.

As an example, we assume the mass density $\rho_0 = 950\,\mathrm{kg\,m^{-3}}$, Young's modulus $E_0 = 8.88\,\mathrm{MPa}$ and Poisson's ratio $\nu_0 = 0.48$ for the rubber slab, as well as the mass density $\rho_1 = 1.23\,\mathrm{kg\,m^{-3}}$, and the wave velocity $c_1 = 343\,\mathrm{m\,s^{-1}}$ for the fluid material (air). The geometric parameters used in the simulation are chosen as $d = 100\,\mathrm{mm}$, $w = 400\,\mathrm{mm}$, and $a = 50\,\mathrm{mm}$.

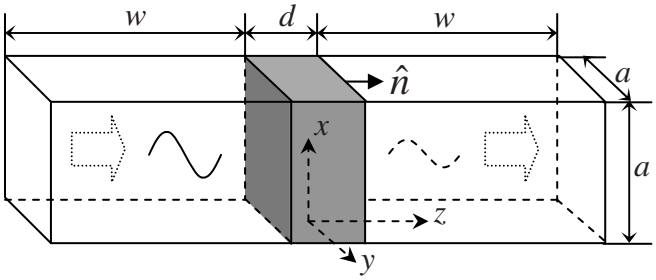

Figure 5. The simulation environment for calculating the sound transmission through a clamped slab.

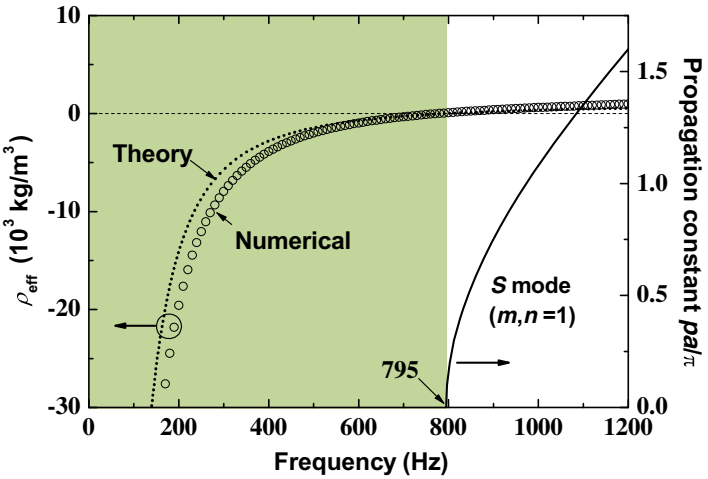

Figure 6. The dispersion curve (pa/π versus frequency) from equation (6) for a square waveguide of dimensions $50 \times 50\,\mathrm{mm}^2$ totally filled with rubber and having clamped boundary conditions, as well as the effective mass density of the clamped rubber slab predicted by the waveguide theory from equation (7) and numerical simulation from equation (8).

Effective mass density ρ'_{eff} for the clamped slab can be defined by homogenizing the equation of motion. Consider the direction $\hat{n}$ of interest, the effective mass density ρ'_{eff} can be defined as

$$\rho'_{\mathrm{eff}} = [\bar{p}]/\bar{u}_{tt}, \tag{8}$$

where $[\bar{p}]$ equals $\bar{p}_1 - \bar{p}_2$, with $\bar{p}_i$ being the pressure integration over the left and right surfaces of the slab, and $\bar{u}_{tt}$ denoting the volume integration of accelerations.

Figure 6 gives the dispersion curve of the square waveguide totally filled with rubber, which is calculated by equation (6). Within the frequency 1200 Hz of interest, one branch is shown up, corresponding to the lowest S mode $(m,n = 1)$. It can be seen from the dispersion curve that a wideband gap is opened below 795 Hz. The effective mass predicted by the waveguide theory (7) is shown in figure 6 by the dotted line, together with numerical prediction (8) given by the circle; good agreement between theoretical and numerical results can be observed, which confirms the negative-mass behavior of the clamped waveguide. According to equation (7), the cut-off frequency $\omega_{\mathrm{c}} = (\sqrt{2}\pi/a)\sqrt{\mu_0/\rho_0}$ that separates the positive and the negative effective

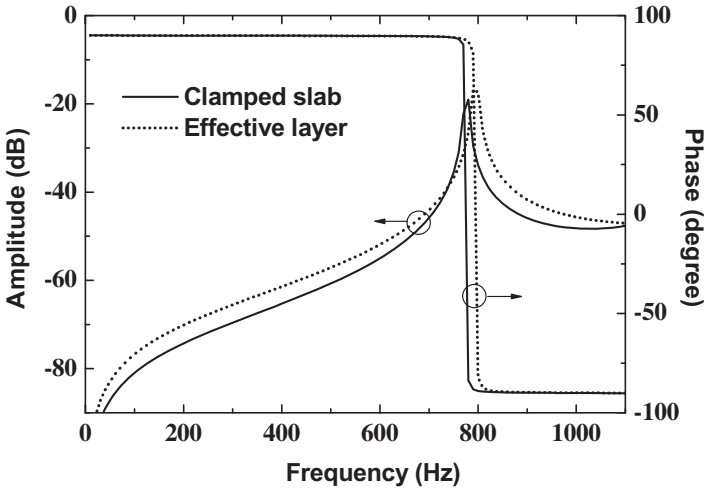

Figure 7. Sound transmission amplitude and phase through the clamped rubber slab and its effective layer with negative-mass density.

mass is associated with the shear modulus of the filling material. This means that stiff materials with high shear modulus can enhance this frequency. If, in contrast, we take the limit $\mu_0 \to 0$, the filling material behaves like a fluid. In this case, the bandgap disappears, recovering the fact that a fluid in a pipe cannot stop sound waves of any frequency.

The transmission amplitude and phase of sound waves across the clamped rubber slab have been calculated and are shown in figure 7 by solid lines. For comparison, the transmission spectra of an effectively homogeneous layer with negative-mass density are given by dotted lines, which is computed from

$$T = \frac{1}{\cos(\omega d/c_{\text{eff}}) + (i/2)\,\sin(\omega d/c_{\text{eff}})\,(z_1/z_{\text{eff}} + z_{\text{eff}}/z_1)}, \tag{9}$$

where $z_1 = \rho_1 c_1$ is the characteristic impedance of air and c_{eff} and z_{eff} are, respectively, the wave velocity and impedance of the longitudinal wave of the homogeneous layer. The effective material is assumed to have the mass density ρ_{eff} given by equation (7), and the Young's modulus and Poisson's ratio are the same as those of the rubber slab $E_{\text{eff}} = 8.88$ MPa and $\nu_{\text{eff}} = 0.48$. For the transmission amplitude and phase good agreement can be observed between the clamped slab and the effective layer.

4. Elastic metamaterials with broadband negative-mass density

In section 3, we demonstrate that an elastic slab with fixed outer boundaries has negative effective mass below a cut-off frequency, and this specific frequency is inversely proportional to the cross-sectional size of the slab. Based on these observations, we propose elastic metamaterials with broadband negative mass, which may be useful for low-frequency noise isolation.

The designed metamaterial is a steel grid filled with styrene butadiene rubber 1502 (SBR), as shown in figure 8. Since a steel grid is much more rigid than rubber, it provides naturally a fixed boundary for the SBR. The proposed metamaterial can be considered to be the parallel

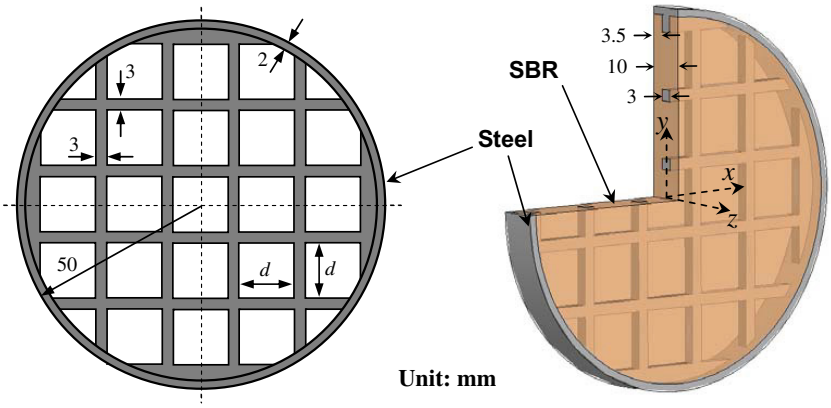

Figure 8. Geometrical sizes of metamaterial samples. (Two samples with $d = 15$ and 10 mm are fabricated.)

stacking of small square waveguides. According to the results given in section 3, we can design the cut-off frequency of negative effective mass by choosing the size of the grid and filling material. Two different gird sizes $d = 15$ and 10 mm are designed. The samples have a circular boundary of diameter 100 mm to facilitate the measurement using a Brüel and Kjær type-4206T impedance tube. The thickness of the sample is 10 mm.

The transmission spectrum of the sample is measured in a Brüel and Kjær type-4206T impedance tube with four microphones. Two microphones in the front tube measure the incident and reflected signals. The other two microphones are placed in the transmission tube and measure transmission signals and the reflected waves from the termination. The standard testing procedure for transmission loss supported by the impedance tube 4206T is followed. Each testing material is tested twice in two different termination conditions, respectively. In our measurement, the transmission tube is terminated by the open end in a quiet background and the sound-absorbing material with good performance. The data acquired from four sensors and two testing results are used to uniquely determine the transfer function [18] of the tested material. From the transfer function, the normal incident transmission spectrum with amplitude and phase can be derived for the ideal case of anechoic termination. In the measurements, the edge of the sample is sealed and fixed on the inner wall of the impedance tube. Two specimens for each sample are fabricated and each specimen is measured twice for sound waves incident on different surfaces. It is found that there are very few discrepancies among measured results.

Figure 9(a) shows the measured transmission amplitudes and phases of the samples with $d = 15$ and 10 mm. From the amplitude curve of the sample of $d = 15$ mm it can be seen that there is a peak transmission around 1108 Hz, below which a significant transmission drop is observed. It will be shown in the following that the drop is due to negative effective mass. Across the transmission peak, the phase is gradually reversed. These features are very similar to those exhibited in figure 7 for a clamped elastic slab, giving an indication of the negative-mass behavior below this specific frequency. Note that from the amplitude curve, one can find a relatively constant transmission from 500 to 700 Hz. The corresponding transmission phase is a little twisted. This behavior is the typical resonant effect in the impedance tube itself due to the imperfection of anechoic termination in practice, and this effect may become more noticeable when the tube is loaded with the fixed sample. One would not observe this resonant effect in

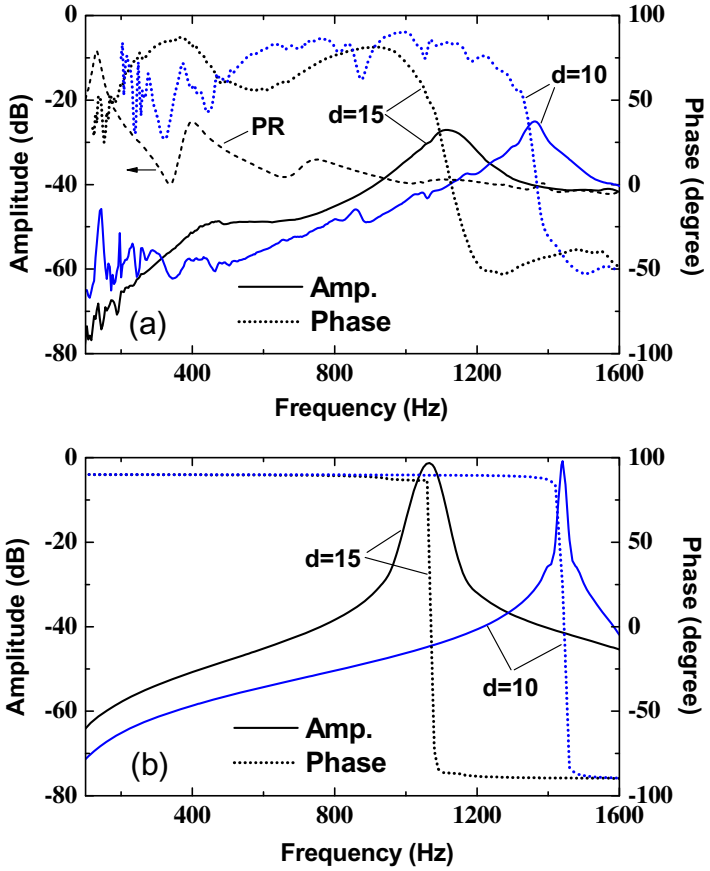

Figure 9. Transmission amplitude and phase: (a) experimental results for samples with grid size $d = 15$ and 10 mm and (b) the corresponding simulation results. The dashed line labeled 'PR' in (a) represents the measured transmission amplitude of the clamped pure rubber slab of diameter 100 mm and thickness 10 mm.

the following simulation results when the non-reflection radiation boundary condition is used, as shown in figure 9(b). However, this effect will not affect the entire profile of the transmission spectrum. For the sample with $d = 10$ mm, the transmission peak occurs at about 1360 Hz and is accompanied by the phase reverse. A resonant effect due to the impedance tube itself now takes place at about 880 Hz, which is weaker than that exhibited by the sample of $d = 15$ mm. The measured results show that the peak transmission frequency is enhanced with decreasing the grid's size, as coincides with the prediction of the waveguide theory. For reference, the transmission amplitude of a clamped pure rubber slab of diameter 100 mm and thickness 10 mm is also given by the dashed line labeled 'PR' in figure 9(a). Due to the large lateral dimension, the lowest eigenfrequency is measured to be as low as 132 Hz, and there are multiple resonant peaks in the frequency range of interest, giving rise to a transmission loss lower than 40 dB. That is why we introduce the rigid grid to produce the wideband cutoff mode and to achieve higher transmission loss.

Figure 9(b) shows the simulation results for sound transmission through the samples with $d = 15$ and 10 mm. The Young's modulus, Poisson's ratio and mass density were measured

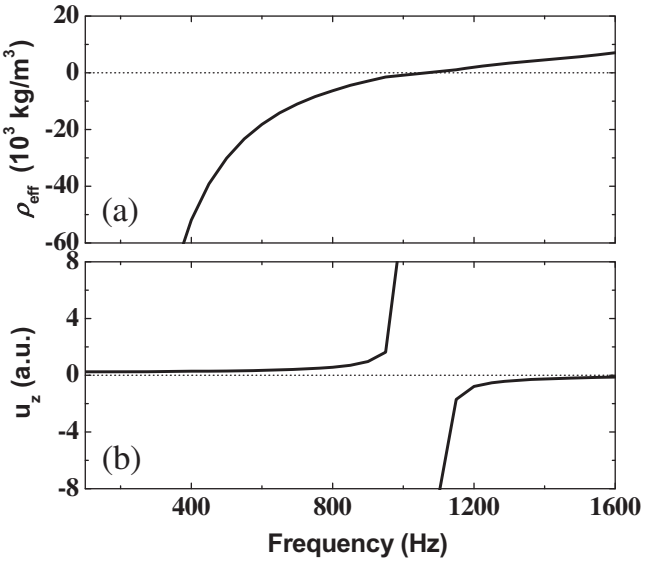

Figure 10. (a) Effective mass density and (b) the averaged displacement u_z of the sample with $d = 15$ mm.

by using uniaxial tension tests to be $E_s = 194$ GPa, $\nu_s = 0.28$ and $\rho_s = 7700\,\mathrm{kg\,m^{-3}}$ for steel and $E_r = 1.88$ MPa, $\nu_r = 0.499$ and $\rho_r = 963\,\mathrm{kg\,m^{-3}}$ for SBR. In the simulation, the damping property of rubber is not taken into account. As a result, some discrepancies exist in the transmission amplitudes between the numerical and the experimental results. The overall trends of the calculated amplitude and phase are in agreement with the experimental results.

In order to understand the transmittance drop when the frequency deviates from the peak transmission frequency, we calculate the effective mass of the sample with $d = 15$ mm according to equation (8) and the averaged displacements in the normal direction to the surface of the sample; the results are shown in figures 10(a) and (b), respectively. It is seen that the cut-off frequency that separates the negative- and positive-mass regions is the lowest eigenfrequency at which the sample undergoes the resonance. Across the resonant frequency, the vibration direction of the sample is reversed, resulting in a phase change in transmission. In the positive-mass region, the transmittance drop is due to the increasing of both frequency and mass density, as governed by the mass law, and also to the fact that the structure does not respond very promptly to external excitations owing to the resonant effect. In the negative-mass band, the propagation constant will be purely imaginary, giving rise to the evanescent wave mode in the sample. The magnitude of negative effective mass increases with decreasing frequency. The decay length of waves in the sample will then be shortened, resulting in the decrease of the transmittance. The transmission drop in the negative-mass band cannot be explained by the mass law. This property is very useful for achieving low-frequency insulations for sounds and vibrations.

Finally, to exclude the possibility that the transmission drop below the cut-off frequency is due to the energy absorption by the sample, figure 11 shows the energy dissipation coefficients α for the samples. In the sound transmission experiment, they are obtained by $\alpha = 1 - |R|^2 - |T|^2$, where R and T are the reflection and transmission coefficients, respectively. Due to the resonant behavior of the sample at the cut-off frequency, there are considerable energy dissipations.

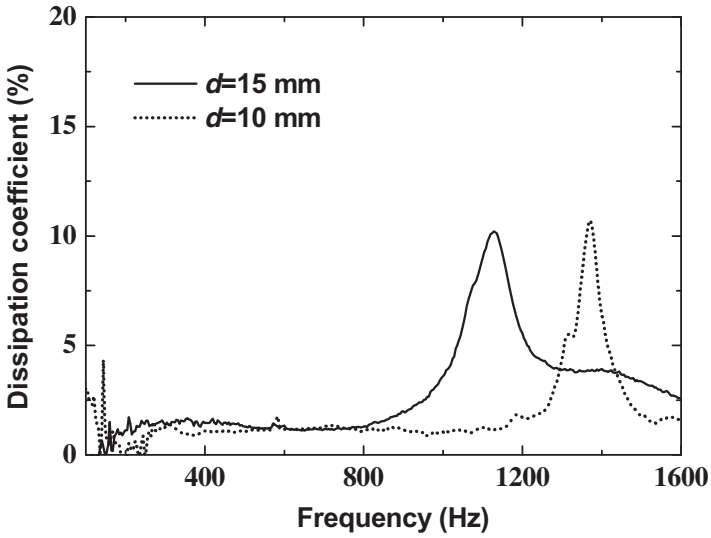

Figure 11. Energy dissipation coefficients for the samples with $d = 15$ and 10 mm measured in sound transmission experiments.

Below this frequency, the energy dissipation rapidly decreases and reaches constant values. The results clearly reveal that the dip in transmission below the cut-off frequency is induced by the reflection due to negative effective mass, not by the energy absorption. As a final remark, since the samples operate in the long-wavelength regime for the case under investigation, it would be better to consider the sample as a single unit of the mass–spring system.

5. Conclusion

Negative-mass behaviors below a cut-off frequency are studied both theoretically and experimentally for different systems. A mass–spring structure is demonstrated to possess negative effective mass below a specific frequency. The transmittances measured in a finite lattice system confirm the negative-mass-induced bandgap. It is found that the additional spring-like forces that act on the mass are the key factor for achieving this peculiar property. For elastic wave propagation in a rectangular waveguide, the peculiar negative-mass effect can be observed by applying the clamped boundary conditions. Analyses of the dispersion relation of the clamped waveguide confirm that the bandgap effect existing below the cut-off frequency can be correlated to negative effective mass. Based on these findings, elastic metamaterials made of steel grids and rubber are designed and fabricated. Both numerical and experimental results show that the proposed metamaterials have negative effective mass below the cut-off frequency.

Similar behaviors would be expected for a clamped waveguide with other shapes of the cross section. From this perspective, one has much flexibility in designing new broadband elastic metamaterials, which pave the way for broadband and low-frequency insulations for sounds and vibrations. Further study can be performed by introducing monopole resonances [13, 19, 20] to produce negative effective modulus, so as to realize left-handed metamaterials. These studies offer potential applications in elastic wave control and seismic wave protection. Our findings may have an interesting correlation with the EM wave phenomenon that a hollow metallic waveguide can be considered as a Drude plasma [6]. The EM waveguide structures can be

utilized to generate surface plasmons [21], as is done by Drude metals such as silver. If a correlation exists between the two phenomena, we may expect new surface modes arising from acoustic metamaterials with effective mass following the Drude relation, which can be used in nondestructive testing.

Acknowledgments

This work was supported by the National Natural Science Foundation of China (10702006 and 10832002) and the National Basic Research Program of China (2006CB601204).

References

[1] Fang N, Lee H, Sun C and Zhang X 2005 *Science* **308** 534
[2] Li J, Fok L, Yin X, Bartal G and Zhang X 2009 *Nature Mater.* **8** 931
[3] Schurig D, Mock J J, Justice B J, Cummer S A, Pendry J B, Starr A F and Smith D R 2006 *Science* **314** 977
[4] Liu R, Ji C, Mock J J, Chin J Y, Cui T J and Smith D R 2009 *Science* **323** 366
[5] Pendry J B, Holden A J, Robbins D J and Stewart W J 1996 *Phys. Rev. Lett.* **76** 4773
[6] Marqués R, Martel J, Mesa F and Medina F 2002 *Phys. Rev. Lett.* **89** 183901
[7] Pendry J B, Holden A J, Stewart W J and Youngs I 1999 *IEEE Trans. Microw. Theory Tech.* **47** 2075
[8] Liu Z Y, Zhang X X, Mao Y W, Zhu Y Y, Yang Z Y, Chan C T and Sheng P 2000 *Science* **289** 1734
[9] Milton G W and Willis J R 2007 *Proc. R. Soc.* A **463** 855
[10] Yao S, Zhou X and Hu G 2008 *New J. Phys.* **10** 043020
[11] Huang H H and Sun C T 2009 *New J. Phys.* **11** 013003
[12] Liu Z, Chan C T and Sheng P 2005 *Phys. Rev.* B **71** 014103
[13] Zhou X M and Hu G K 2009 *Phys. Rev.* B **79** 195109
[14] Yang Z, Mei J, Yang M, Chan N H and Sheng P 2008 *Phys. Rev. Lett.* **101** 204301
[15] Yang Z, Dai H M, Chan N H, Ma G C and Sheng P 2010 *Appl. Phys. Lett.* **96** 041906
[16] Lee S H, Park C M, Seo Y M, Wang Z G and Kim C K 2009 *Phys. Lett.* A **373** 4464
[17] Miklowitz J 1978 *The Theory of Elastic Waves and Waveguides* (New York: North-Holland)
[18] Chung J Y and Blaser D A 1980 *J. Acoust. Soc. Am.* **68** 907
[19] Li J and Chan C T 2004 *Phys. Rev.* E **70** 055602
[20] Ding Y Q, Liu Z Y, Qiu C Y and Shi J 2007 *Phys. Rev. Lett.* **99** 093904
[21] Pendry J B, Martin-Moreno L and Garcia-Vidal F J 2004 *Science* **305** 847